Long-term memory in experiments and numerical simulations of hydrodynamic and magnetohydrodynamic turbulence

Pablo Mininni, Pablo Dmitruk, Philippe Odier, Jean-François Pinton, Nicolas Plihon, Gautier Verhille, Romain Volk, Mickaël Bourgoin

▶ **To cite this version:**

Pablo Mininni, Pablo Dmitruk, Philippe Odier, Jean-François Pinton, Nicolas Plihon, et al.. Long-term memory in experiments and numerical simulations of hydrodynamic and magnetohydrodynamic turbulence. Physical Review E : Statistical, Nonlinear, and Soft Matter Physics, 2014, Physical Review E, 89, pp.053005. 10.1103/PhysRevE.89.053005 . hal-01140470

HAL Id: hal-01140470
https://hal.science/hal-01140470

Submitted on 8 Apr 2015

HAL is a multi-disciplinary open access archive for the deposit and dissemination of scientific research documents, whether they are published or not. The documents may come from teaching and research institutions in France or abroad, or from public or private research centers.

L'archive ouverte pluridisciplinaire **HAL**, est destinée au dépôt et à la diffusion de documents scientifiques de niveau recherche, publiés ou non, émanant des établissements d'enseignement et de recherche français ou étrangers, des laboratoires publics ou privés.

Long-term memory in experiments and numerical simulations of hydrodynamic and magnetohydrodynamic turbulence

P. Mininni,[1] P. Dmitruk,[1] P. Odier,[2] J.-F. Pinton,[2] N. Plihon,[2] G. Verhille,[3] R. Volk,[2] and M. Bourgoin[4]
[1]*Departamento de Física, Facultad de Ciencias Exactas y Naturales, Universidad de Buenos Aires and IFIBA, CONICET, Ciudad Universitaria, 1428 Buenos Aires, Argentina*
[2]*Laboratoire de Physique - UMR 5672 Ecole Normale Suprieure de Lyon / CNRS 46 Allée d'Italie, 69007 Lyon, France*
[3]*Aix-Marseille Université, IRPHE - UMR 7342, CNRS, Marseille, France*
[4]*Laboratoire des Écoulements Géophysiques et Industriels, UMR5519 CNRS/UJF/Grenoble-INP/Université de Grenoble, BP53, 38041, Grenoble cedex 9, France*
(Received 22 January 2014; published 8 May 2014)

We analyze time series stemming from experiments and direct numerical simulations of hydrodynamic and magnetohydrodynamic turbulence. Simulations are done in periodic boxes, but with a volumetric forcing chosen to mimic the geometry of the flow in the experiments, the von Kármán swirling flow between two counterrotating impellers. Parameters in the simulations are chosen to (within computational limitations) allow comparisons between the experiments and the numerical results. Conducting fluids are considered in all cases. Two different configurations are considered: a case with a weak externally imposed magnetic field and a case with self-sustained magnetic fields. Evidence of long-term memory and $1/f$ noise is observed in experiments and simulations, in the case with weak magnetic field associated with the hydrodynamic behavior of the shear layer in the von Kármán flow, and in the dynamo case associated with slow magnetohydrodynamic behavior of the large-scale magnetic field.

DOI: 10.1103/PhysRevE.89.053005 PACS number(s): 47.65.−d, 47.27.−i

I. INTRODUCTION

Since the development of hot-wire measurements in hydrodynamic turbulence in the laboratory, several reports of long-term memory in velocity time series (i.e., nonnegligible correlations in time scales much larger than the time scale associated with the energy-containing eddies in the flow) can be found in the literature (see, e.g., [1,2] for recent reports). The origin of such long-term correlations is unclear, as current knowledge of turbulence indicates that three-dimensional flows should transfer energy from the energy-containing scale towards smaller scales (where the characteristic time scales are shorter). Therefore, no correlations at time scales longer than the energy-containing scale are to be expected.

Evidence of long-term memory (or "long-range dependence") is often observed in the frequency spectrum of time series as a range of frequencies corresponding to $1/f$ noise. By $1/f$ noise (also often called "flicker" noise), it is usually meant that the power spectrum of the signal is of the form $E(f) \sim f^{-\alpha}$, where f is the frequency, and with α loosely between 0.5 and 1.5. The case with $\alpha = 1$, which strictly speaking corresponds to $1/f$ noise, is the case with equal energy per octave independent of the frequency. The range of frequencies in which this phenomenon often develops corresponds not only to frequencies smaller than the frequency associated with the energy-containing eddies, but often also to frequencies that (if the Taylor hypothesis is used) are associated with length scales much larger than the physical extension of the fluid. Therefore, such correlations cannot be associated with convective motions in the turbulent flow, and must be associated with long-term modulations in the system.

Observations of $1/f$ fluctuations are not exclusive of hydrodynamic or magnetohydrodynamic (MHD) turbulence, and are widely found in natural and nonlinear systems [3]. As a result, they are often considered as a signature of scale-invariant features of an underlying dynamical process. Time signals displaying $1/f$ noise in their spectral density have been reported in electronics, tree growth, and human activities such as music and the stock market [4]. In conducting fluids and plasmas, $1/f$ fluctuations have also been reported (see, e.g., [5,6]). In the interplanetary magnetic field, its presence has been known for some time through analysis of time signals measured *in situ* near Earth's orbit [7–9]. Long-term behavior has also been found in time series of the geomagnetic field [10–12] and in dynamo laboratory experiments [13].

This ubiquity has motivated several works that attempted to identify general sources of $1/f$ noise and long-term memory. Recent studies focused in the particular cases of hydrodynamic and MHD flows [6,14] obtained $1/f$ in MHD with and without a background magnetic field, but did not observe it in isotropic hydrodynamic flows. The modes giving the dominant contribution to the long-term correlations were identified to be modes with the largest available wavelength in the domain. Random isotropic forcing, with a short-time memory to give a single (unit) correlation time, was used to stir the flows in [6], while random initial conditions in ideal systems were considered in [14]. It was concluded that long-term memory is more easily seen in systems that develop inverse cascades, or that have nonlocal interactions [15].

In this work, we consider time series stemming from experiments and direct numerical simulations of hydrodynamic and MHD turbulence. Simulations are done in periodic boxes, but with a volumetric forcing chosen to mimic the geometry of the flow in the experiments. Parameters in the simulations are also chosen to (within computational limitations) allow comparisons between the experiments and the numerical results. Two different configurations are explored: the case with an externally imposed magnetic field (but with the magnetic field weak enough that can be considered a passive vector

 ©2014 American Physical Society

tracer and used to characterize the flow), and the case with self-sustained magnetic fields. The former case (corresponding to "induction," as the magnetic field fluctuations observed are induced by motions of the conducting flow) can be relevant for many liquid metal laboratory experiments and for industrial flows. The latter, corresponding to a magnetohydrodynamic dynamo, has implications for magnetic field generation in geophysics and astrophysics.

II. EXPERIMENTS AND SIMULATIONS

A. Experiments

Experimental data discussed in this article have been obtained in the VKG and VKS experimental setups (see Fig. 1). The VKG experiment is a von Kármán swirling flow of liquid gallium, while VKS is a von Kármán flow of liquid sodium. In both cases the von Kármán flow is generated in the gap between two counterrotating impellers in a cylindrical vessel. This geometry has been extensively investigated in the past decade in the context of magnetic field self-generation by dynamo effect. Its interest in MHD studies has been motivated by the large-scale topology of the generated flow which exhibits strong differential rotation and helicity.

The VKG experiment is mostly designed to investigate MHD mechanisms as induction processes (transport and deformation of magnetic field lines by the flow) and flow modification by an imposed magnetic field (via the Lorentz force acting on the moving conducting fluid). The reachable magnetic Reynolds number $\mathrm{Rm} = UL/\eta$ (which compares the magnetic induction effects to magnetic dissipation effects, with U the typical velocity of the flow, L its typical dimension, and η the magnetic diffusivity) accessible in VKG is of order unity so that no dynamo effect is expected to be observed in this experiment. On the other hand, the VKS facility has been designed and optimized for dynamo generation. It is twice as large as VKG, with an available mechanical power 15 times larger, and it uses liquid sodium which is less resistive than gallium. As a consequence, the accessible magnetic Reynolds number in VKS is of the order of 50. In 2006 the first dynamo generation was observed in VKS when soft iron-impellers were used to drive the flow. Details of the VKG and VKS experiments can be found in [13,16,17].

As for all liquid metals, the magnetic Prandtl number (defined as the ratio of the kinematic viscosity ν of the fluid to its magnetic diffusivity η, $\mathrm{Pm} = \nu/\eta$) of gallium and sodium is very small ($\mathrm{Pm}^{\mathrm{Ga}} = 1.4 \times 10^{-6}$, $\mathrm{Pm}^{\mathrm{Na}} = 6.2 \times 10^{-6}$). As a consequence, flows with magnetic Reynolds number Rm of order unity or larger have a kinematic Reynolds number $\mathrm{Re} = UL/\nu = \mathrm{Rm}/\mathrm{Pm}$ exceeding 10^5, hence operating in highly turbulent conditions. Magnetic processes in VKG and VKS experiments are therefore submitted to highly fluctuating turbulent flows. To this respect, von Kármán flows are particularly interesting as they are known to present a wide hierarchy of scales of fluctuations. At intermediate and small scales, the flow behaves as *traditional* turbulence (although anisotropic), with for instance a classical $k^{-5/3}$ Kolmogorov spatial spectra. At larger scales the flow undergoes in many cases long-term dynamics, which in the absence of strong or

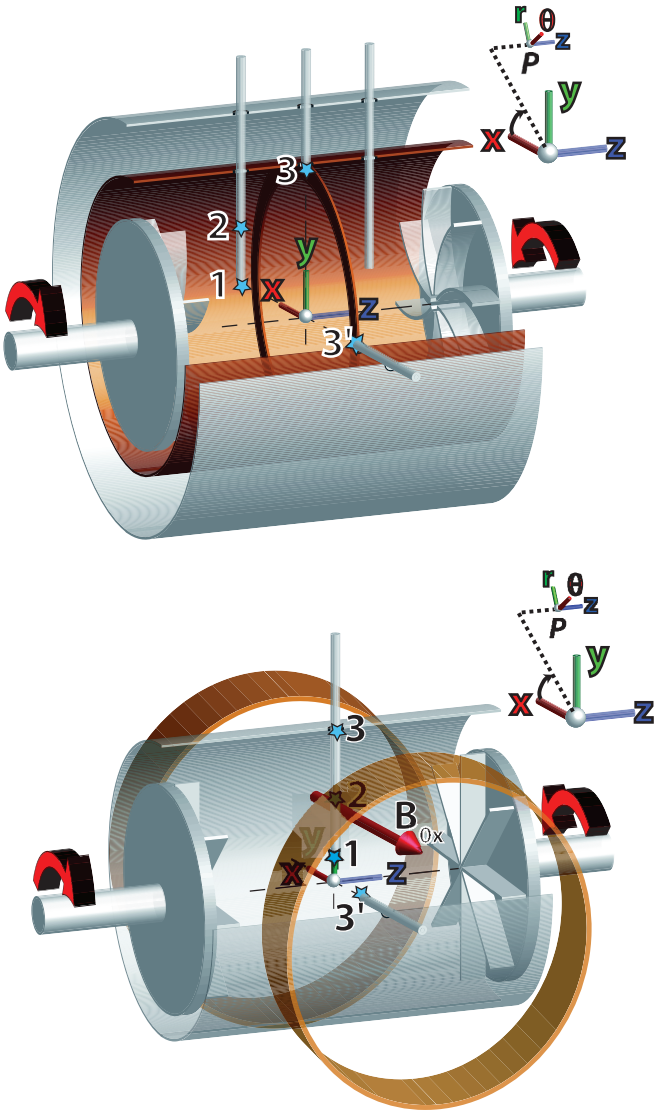

FIG. 1. (Color online) Sketch of the experimental setups. (a) VKS experiment drives a von Kármán swirling flow of liquid sodium in a cylindrical vessel. Data from the experiments reported here were obtained in a configuration with an inner copper shell and an annulus in the midplane. (b) VKG experiment drives a von Kármán flow of liquid gallium in a cylindrical vessel. A pair of lateral Helmholtz coils allows us to apply a transverse magnetic field. Positions of the measurement probes are indicated with the stars.

self-generated magnetic fields are mostly driven by hydrodynamic instabilities of the midplane shear layer [2,18].

As already mentioned, the VKG experiment is meant to investigate magnetohydrodynamic induction processes with magnetic Reynolds number $\mathrm{Rm} < 1$. To this purpose a pair of transverse coils is placed laterally to the experiment and allows us to apply a transverse magnetic field B_{0x}. When the applied magnetic field is sufficiently weak so that the interaction parameter $N = \mu_0 L B_{0x}^2/\eta\rho U$ remains low and of the order of 10^{-3}, the imposed magnetic field can be considered as a passive vector, advected by the flow. Recent experiments [19] have shown that this approximation stops being valid as soon as $N \geq N^* \approx 0.02$, in which case the flow itself is modified

by the applied magnetic field. Only the situation in which the magnetic field is weak and acts as a passive vector will be considered here. In this case, the magnetic field can just be used as a way to measure and characterize the hydrodynamic flow.

The VKS experiment has several possible configurations. We will focus here on the geometry sketched in Fig. 1 (top), which has been extensively investigated and for which the main results have been reported in Ref. [13]. The flow is driven with iron impellers, such that a self-sustained dynamo magnetic field is observed above a magnetic Reynolds number threshold of the order of $\mathrm{Rm}^c \approx 30$.

Accessible measurements in VKS and VKG are mainly magnetic, as well-resolved velocimetry is extremely difficult in liquid metals, though some kinematic measurements have been recently made accessible thanks to a local miniature Vivès probe [20]. The induced or self-sustained magnetic field is measured inside the flow by means of Hall probes. In the VKG experiments, measurements were accessible on a line along the vertical Oy axis in the midplane (see the numbered stars in the bottom panel of Fig. 1); few measurements along the Ox axis in the midplane are also available. In the VKS experiments, measurements were accessible at the locations indicated by stars in Fig. 1 (top).

B. Numerical simulations

The numerical simulations solve the equations for an incompressible flow in a three-dimensional periodic domain of side 2π. In the most general case (a conducting fluid with an externally imposed magnetic field of strength $\mathbf{B}_0$), the equations in dimensionless Alfvénic units read

$$\frac{\partial \mathbf{u}}{\partial t} + \mathbf{u}\cdot\nabla\mathbf{u} = -\nabla\mathcal{P} + \mathbf{j}\times(\mathbf{b}+\mathbf{B}_0) + \nu\nabla^2\mathbf{u} + \mathbf{F}, \quad (1)$$

$$\frac{\partial \mathbf{b}}{\partial t} + \mathbf{u}\cdot\nabla\mathbf{b} = (\mathbf{b}+\mathbf{B}_0)\cdot\nabla\mathbf{b} + \eta\nabla^2\mathbf{b}. \quad (2)$$

In the incompressible case $\nabla\cdot\mathbf{u}=0$, and $\nabla\cdot\mathbf{b}=0$. Here, $\mathbf{u}$ is the velocity, $\mathbf{b}$ is the magnetic field, and $\mathbf{j}=\nabla\times\mathbf{b}$ is the current density. The pressure (normalized by the density) is $\mathcal{P}$, $\nu = 4.7\times10^{-3}$ is the dimensionless kinematic viscosity, and η the magnetic diffusivity, with $\eta=\nu/\mathrm{Pm}$. In the absence of an externally imposed magnetic field ($\mathbf{B}_0=0$) these equations are the incompressible MHD equations often used to study the dynamo effect. When $\mathbf{B}_0=\mathbf{b}=0$ (or when the interaction parameter N is small enough), Eq. (1) reduces to the Navier-Stokes equation for an incompressible hydrodynamic flow.

To mimic the geometry of the flow in the experiment, a Taylor-Green (TG) vortex is used as mechanical forcing

$$\mathbf{F} = A_0\begin{bmatrix}\sin(k_0x)\cos(k_0y)\cos(k_0z)\\ -\cos(k_0x)\sin(k_0y)\cos(k_0z)\\ 0\end{bmatrix}, \quad (3)$$

where $A_0=0.41$ is the forcing amplitude, and $k_0=2$ is the forcing wave number. This forcing was shown before to give good agreement with von Kármán dynamo results [21,22], while allowing simulations to be done in periodic boundaries and thus lowering computational costs. A sketch of the resulting flow in one TG cell can be seen in Fig. 2.

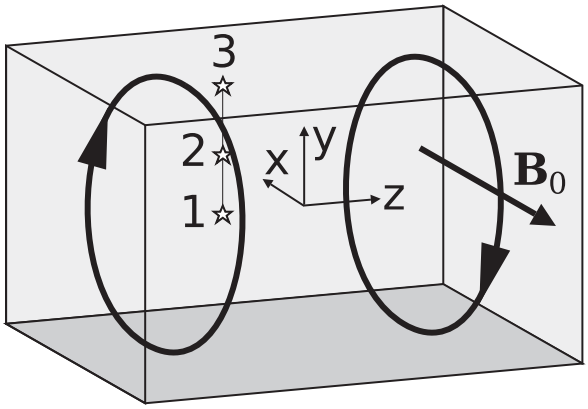

FIG. 2. Sketch of the numerical Taylor-Green cell, and position of the points where magnetic and velocity measurements are made (indicated with stars). The two large circular arrows represent the two counterrotating Taylor-Green vortices.

The forcing is applied at $k_0=2$ as in the dynamo case the magnetic field grows at a scale larger than the flow energy containing scale. Forcing at $k_0=1$ would result in a suppression of that dynamo eigenmode, resulting in a different eigenmode of the kinematic dynamo being artificially excited and in differences in the spatial structure of the magnetic field when compared with experiments (see [22]). Note however that applying the force at $k_0=1$ or 2 does not introduce differences in the slow dynamics of the hydrodynamic flow, as the slow dynamics takes place at time scales much longer than the turnover time of the energy-containing eddies.

Equations (1) and (2) are solved pseudospectrally using a parallelized code [23–25] dealiased with the 2/3 rule. Second-order Runge-Kutta is used to evolve the equations in time. Since long integrations are needed (in many cases simulations were continued for over 6000 turnover times), linear spatial resolution is $N_{\mathrm{res}}=128$ in all cases. To compare with experiments, time series of the three Cartesian components of the velocity and the magnetic fields at the three points indicated in Fig. 2 are recorded with high cadence. Also, time series of the amplitude and phase of each Fourier mode in spectral space are stored, to be able to identify the modes responsible for long-term behavior. Note that with the spatial resolution considered here, magnetic Reynolds numbers similar to the ones in the experiments are easily reproduced. However, the mechanical Reynolds numbers in the experiments are out of reach for even the largest resolutions we could attain in simulations, and those resolutions would preclude the long-time integrations considered in this study. These choices result in frequency spectra that are well resolved, although spatial resolution in the simulations is only moderate. For a detailed study of wave number spectra at higher spatial resolution under Taylor-Green forcing, see [22].

The strategy used in the simulations is as follows. The mechanical force is turned on at $t=0$ from the flow at rest, and the Navier-Stokes equations (with the $\mathbf{b}$ and $\mathbf{B}_0$ fields set to zero) are advanced for over 6000 turnover times (a turbulent steady state is reached shortly after 10 turnover times). Time series of the velocity are then used for the analysis of $1/f$ noise in hydrodynamic flows (as well as to compare with the equally

long simulations with a weak imposed magnetic field). Later, the last state of the hydrodynamic flow is used to start two different sets of simulations: one in which a uniform magnetic field $\mathbf{B}_0 = B_0\hat{y}$ is imposed, and one in which $\mathbf{B}_0 = 0$ and an initially small magnetic seed is amplified until an MHD steady regime is reached. The former is intended to mimic induction experiments with a transverse magnetic field in VKG, while the latter is intended to mimic dynamo experiments in VKS. In both cases the systems are integrated for over 6000 turnover times. The magnetic Prandtl number in induction simulations is $\mathrm{Pm} = 0.05$ and the interaction parameter is adjusted by setting B_0 such that $N \approx 10^{-4}$. In dynamo simulations $\mathrm{Pm} = 0.5$ as a larger magnetic Reynolds number is needed to sustain magnetic fields [21,22]. The mechanical Reynolds number is fixed in all simulations, and is $\mathrm{Re} = u_{\mathrm{rms}}L/\nu \approx 670$ (with u_{rms} the root mean square velocity in the simulations, and L the integral scale of the flow).

III. HYDRODYNAMIC TURBULENCE AND LOW-N INDUCTION

When the imposed magnetic field is weak enough that it can be considered a passive vector, time series of the velocity field measured in the experiments and simulations at any of the points indicated in Figs. 1 and 2 do not show clear long-term behavior or $1/f$ noise, as can be seen for instance from the dashed lines in Figs. 3 (top) and 4, which represent the kinetic spectra for the simulation and the experiment, respectively. A relatively clear inertial range of time scales, consistent with a classical $f^{-5/3}$ Kolmogorov spectrum, is present, but no significant long-term dynamics is observed at low frequencies, and the spectra flatten rapidly below the forcing frequency F_0 (in the experiment F_0 is taken as Ω, the rotation rate of the impellers, while in the simulation F_0 is determined as u_{rms}/L, where $L = 2\pi/k_0 = \pi$ is the forcing scale and u_{rms} is the root mean square of the turbulent velocity fluctuations).

The absence of long-term dynamics is in agreement with previous results indicating that isotropic and homogeneous hydrodynamic turbulence does not display $1/f$ noise [6]. However, and unlike the results in Ref. [6], when in the numerical simulations the time series of the amplitude of individual Fourier modes are considered, we find that modes in the $k = 1$ shell do have $1/f$ spectra (the observed spectrum is actually steeper than $1/f$; see the bottom panel of Fig. 3).

In the spectra in Fig. 3, note that frequencies with $f/F_0 \leqslant 1$ satisfy the Taylor hypothesis: these frequencies can be converted to wave numbers using the characteristic mean flow velocity. However, for the frequencies with $f/F_0 \lesssim 1$ the Taylor hypothesis does not hold. As an example, for $u_{\mathrm{rms}} \approx 1$ in the simulations, and a length of 2π (the size of the largest eddies that can be excited in the numerical domain), fluctuations with frequencies smaller than $f/F_0 = 0.5$ cannot be associated with any spatial fluctuation, as they correspond to scales larger than the box size. These slow fluctuations are associated with modulations and a long-term memory in the dynamics of the largest eddies.

Interestingly, it can be noted that the modes in the $k = 1$ Fourier shell break down the symmetries of the TG flow and, as an example, are responsible for large-scale fluctuations in the z position of the shear layer between the two Taylor-Green vortices. Indeed, $1/f$ spectra are only observed in modes that break down this symmetry. The spectrum of the temporal fluctuations of small-scale modes (large wave numbers) does not exhibit any long-term dynamics, as can be seen in Fig. 3 (bottom). However, at least at the Reynolds number considered in the simulation, the modes that break down the symmetry do not have enough energy to give rise to a clear long-term

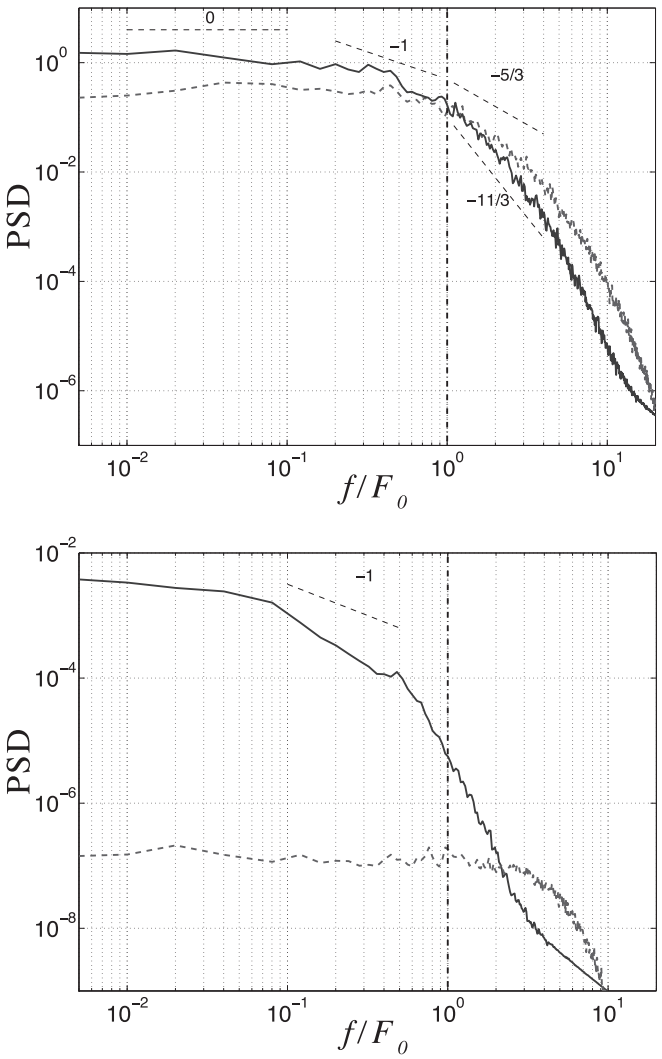

FIG. 3. Numerical simulations of Taylor-Green MHD induction. Top: Power spectrum of the temporal fluctuations of the axial velocity u_z at point 1 (light gray dashed line) and of the axial induced magnetic field (dark gray solid line) in the numerical simulations at low magnetic Prandtl number ($\mathrm{Pm} = 0.05$) and low interaction parameter $N = 4 \times 10^{-5}$. Frequency axis has been normalized by the forcing frequency $F_0 = u_{\mathrm{rms}}/\pi$. The global energy level of the spectra has been arbitrarily set to make them coincide for $f = F_0$. Bottom: Power spectrum of the amplitude of Fourier mode $k = (10,10,10)$ of u_z (light gray dashed line) and of Fourier mode $k = (1,0,0)$ of u_z (dark gray solid line). Note that incompressibility condition imposes the mode $k = (0,0,1)$ of u_z to vanish, while symmetries of the TG flow impose the mode $k = (0,1,0)$ to be identical to the mode $k = (1,0,0)$ shown in the figure. In both panels, several slopes reported before in the VKS and VKG experiments are shown as references, although we are mostly interested in the behavior for $f < F_0$.

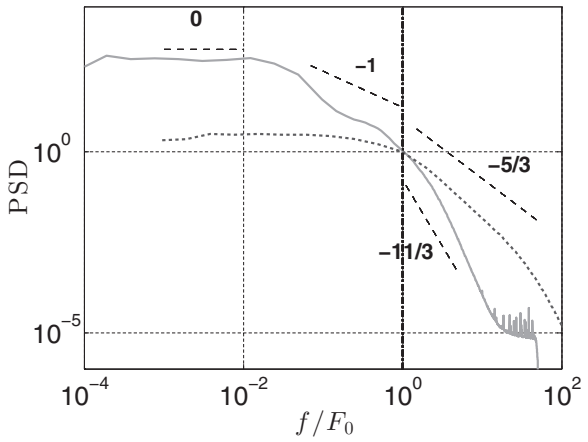

FIG. 4. Experiments of MHD induction in VKG flow. Power spectrum of the axial velocity (light gray dashed line) and of the induced axial magnetic field in VKG experiment with a weak imposed transverse magnetic field (light gray solid line). Frequency axis has been normalized by the forcing frequency F_0 taken as the rotation rate of the impellers Ω (10 Hz for the shown experiment). The total energy level of each spectrum has been normalized by its value at $f/F_0 = 1$. Several slopes are shown as references.

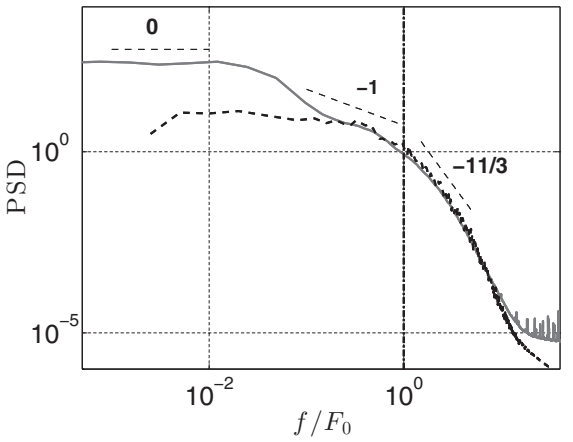

FIG. 5. Experiments vs simulations (induction case): comparison of the spectra of the induced magnetic field in Figs. 3 (simulation, black dashed line) and 4 (experiment, light gray solid line). The total energy level of each spectrum has been normalized by its value at $f/F_0 = 1$. Slopes are shown as references. Measurements from the simulation and the experiment agree remarkably well except for very low frequencies.

behavior when all Fourier modes are integrated to obtain the velocity at one of the measurement points (as shown in the top panel of Fig. 3).

As already mentioned, when modes with $1/f$ behavior are not the most energetic, $1/f$ behavior is not observed in global quantities. However, as soon as a physical effect makes these modes dominant, $1/f$ noise arises. This can be observed for instance by considering the evolution of the small imposed magnetic field with low magnetic Prandtl number and low interaction parameter ($N \ll 1$). Condition $N \ll 1$ ensures that the magnetic field passively traces the carrier velocity field, while condition $\mathrm{Pm} \ll 1$ imposes a large scale separation between magnetic and velocity field, so that only large scales of the velocity field are traced by the magnetic field. Figure 3 (top) also shows the spectrum of the axial induced magnetic field, in the presence of a small applied transverse field, from the numerical simulation (with $\mathrm{Pm} = 0.05$ and $N = 4 \times 10^{-5}$). A short but still visible $1/f$ regime appears for frequencies below the forcing frequency F_0. As previously noted, this regime is not visible for the velocity spectrum. For the comparison, the global energy level of the kinetic and magnetic spectra has been set so as to make them coincide at $f = F_0$.

Similarly, Fig. 4 shows the spectrum of the velocity measured in VKG experiment with a Vivès probe compared to the spectrum of the induced axial magnetic field (measured at point 1) when a weak passive transverse magnetic excitation B_{0x} is imposed (note that the high-frequency resolution of the Vivès probe is limited by magnetic diffusion at the probe size, which is responsible for the cutoff observed here for frequencies $f \gtrsim 200$ Hz [20]). For comparison, the global energy level of the kinetic and magnetic spectra has been set so as to make them coincide at $f = F_0$. Contrary to the kinetic spectrum, the magnetic one shows an important long-term dynamics below F_0 that, in light of the previous numerical observations, shall be attributed to the large-scale modes of the kinetic field naturally traced by the magnetic field in such a low magnetic Prandtl number regime. In other words, the passive magnetic field at very low Pm acts as a low-pass filter that only senses the velocity field at very large scales.

To push further the comparison between the experiment and the simulation, Fig. 5 shows the magnetic spectra from the simulation and the experiment in Figs. 3 and 4 (*axial* component of the induced magnetic field measured at point 1 in the simulation and at point 1 in VKG, which corresponds to the closest available geometries between experiments and simulations). The total energies have been rescaled so that the spectra in the numerics and in the experiment are equal for $f = F_0$. We recall that the frequency axis has been normalized by the corresponding forcing frequency F_0: $F_0 = u_{\mathrm{rms}}/\pi$ for the simulation, and $F_0 = \Omega$ the rotation rate of the disks for the experiment. Interestingly, this scaling was found to give the best collapse between numerics and experiment. As can be seen in the figure, the agreement is indeed remarkable, except for the very low frequencies which are enhanced in the experiment. The slow $1/f$ dynamics for frequencies $f \lesssim F_0$ is in particular observed in both studies. It is also interesting to note that this agreement for the dynamical features of the induction processes is observed even if the dominant induction mechanisms are different in the numerics and the experiment. It has indeed been shown in the experiment that the *mean* axial component induced at the location of the measurement point 1 when a transverse field B_{0x} is applied results from a boundary condition effect due to conductivity difference between the wall of the experiment and the fluid, combined with the presence of local flow vorticity in the vicinity of the boundary [26] (BC mechanism). Such a mechanism cannot be present in the numerics where the entire medium has a homogenous conductivity. This may explain the difference between the simulation and the experiment at very low frequencies, which

in the experiment are dominated by these very specific average induction processes.

However, in both cases the fluctuations of induction processes do trace back the fluctuations of the flow. The long-term effects at $f \lesssim F_0$ for intermediate frequencies must therefore be associated with fluctuations in the velocity field that are present in both the experiments and simulations. In other words, the remarkable collapse of numerical and experimental spectra for moderate and high frequencies indicates that the magnetic field fluctuations at these frequencies are tracing fluctuations of the velocity field with a common origin.

The numerical observation that $1/f$ is essentially related to large-scale hydrodynamic modes breaking the symmetries of the TG flow and the experimental observation of a $1/f$ regime in a configuration where one of the sources of induction is related to radial vorticity in the midplane both point toward an important role (for intermediate frequencies) of the fluctuations of the strong shear layer in the midplane of the von Kármán flow. This shear layer is indeed known to undergo strong large-scale and long-term fluctuations in experimental von Kármán flows [2,18,27]. These fluctuations are also observed in the simulation, and are shown in Fig. 6, which represents the time series of the position of the shear layer as a function of time, and its power spectrum in the numerics. To identify the position of the shear layer in the simulations, a low-pass filtered and averaged (in x and y) velocity field was computed in the TG cells from the Fourier coefficients of the velocity, leaving mean profiles for the azimuthal and z component of the velocity field that depend only on z (see Fig. 2).

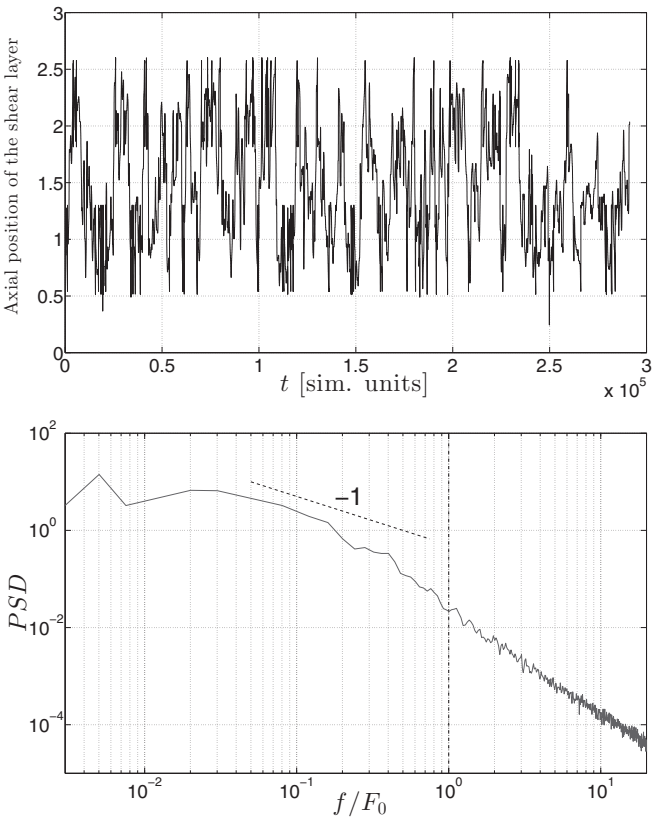

FIG. 6. Numerical simulations. Top: position of the shear layer as a function of time (in simulation units). Bottom: power spectrum of the signal in the top figure. A slope of -1 is indicated as a reference.

In the VKG experiments, a proxy of the evolution of the shear layer can be obtained from measurements of magnetic induction. A particularly clear tracing of the shear layer is obtained when measuring the induced axial magnetic field B_x^i at a location on the horizontal Ox axis (point $3'$ in Fig. 1) for an applied transverse magnetic field B_{0x}. Simple symmetry considerations impose indeed that the induced axial magnetic field measured at any point of the Ox axis for an applied transverse field B_{0x} be zero on average [28]. Figure 7 (top) shows the corresponding time series which clearly shows that the measured signal does fluctuate around zero, but that it explores induction regimes with symmetric polarities which can be attributed to slow symmetry breaking fluctuations of the shear layer respective to its equilibrium position in the midplane [28]. Figure 7 (bottom) shows the corresponding spectrum which does exhibit a clear long-term $1/f$ regime.

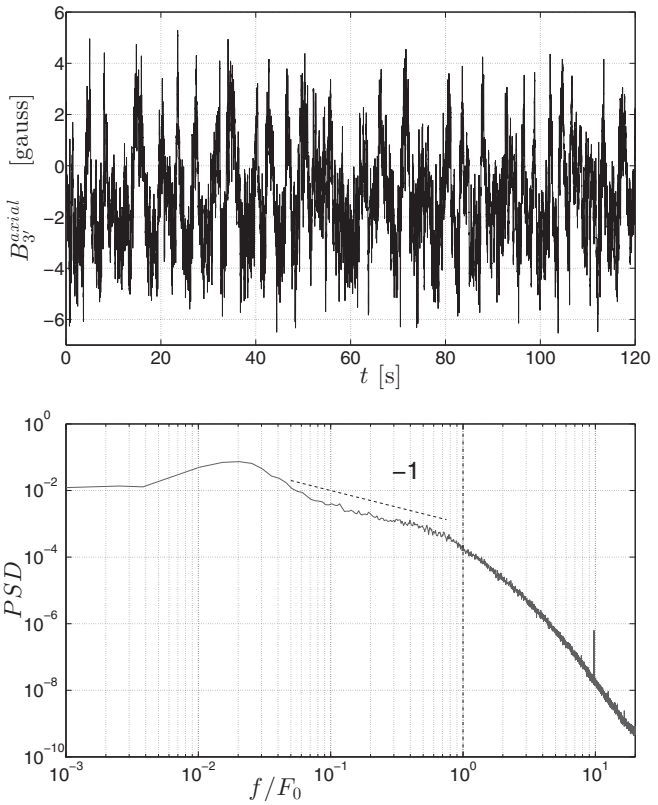

FIG. 7. VKG experiment. Top: proxy of the evolution of the shear layer as a function of time, as indicated by the evolution of the axial induced magnetic field measured at point $3'$. By $\mathcal{R}_\pi$ symmetry around the Ox axis, this component of induced field must be zero. However, it is visible from the measurements that it fluctuates between a high level state (of order 4 gauss) and a low level state (of order -4 gauss). We interpret these fluctuations as a signature of the instantaneous breaking of the $\mathcal{R}_\pi$ symmetry due to the motion of the shear layer. Bottom: power spectrum of the signal in the top figure. A slope of -1 is indicated as a reference.

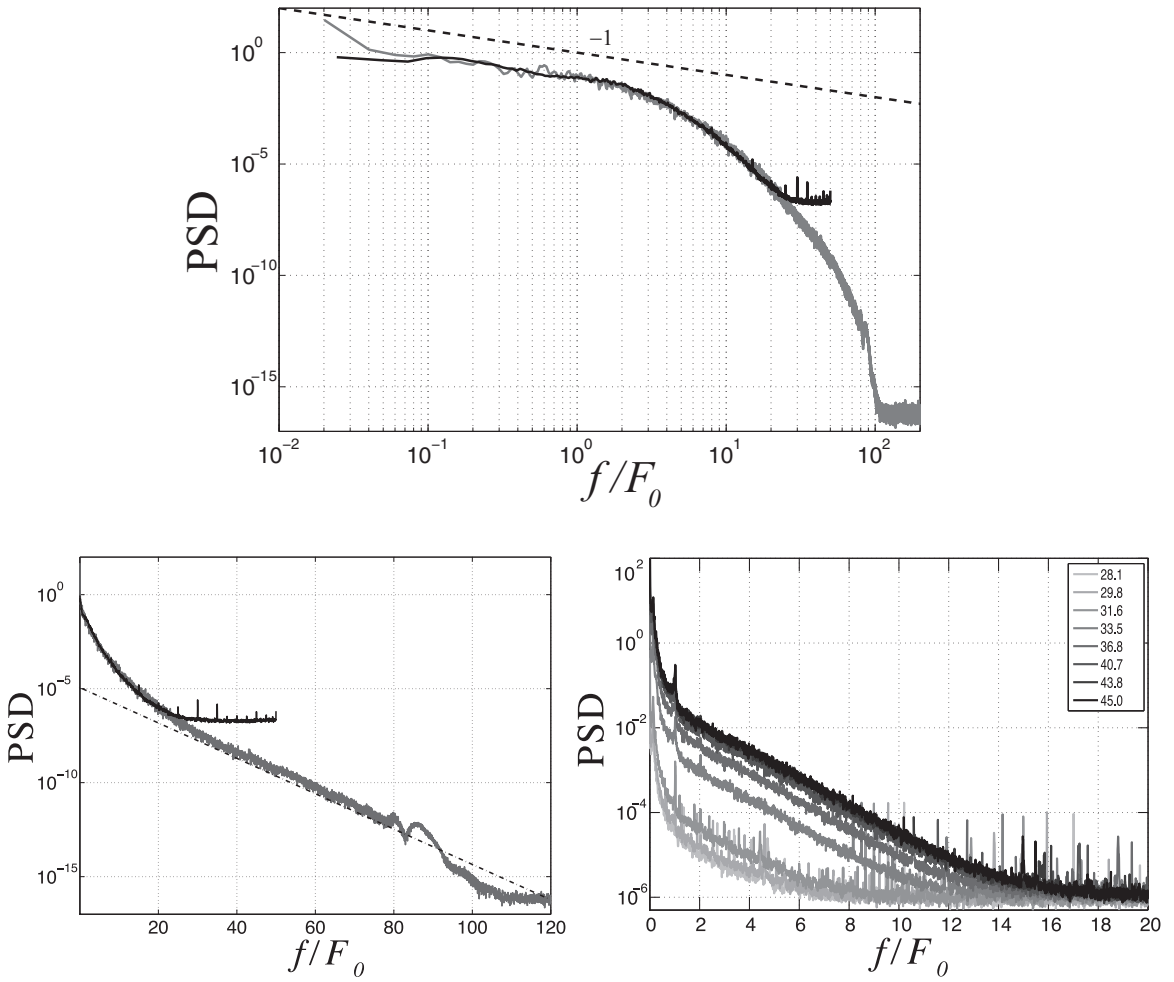

FIG. 8. Experiments vs simulations in the dynamo case. Top: power spectra of the self-sustained magnetic field in the VKS experiment (black) and in the simulation (gray). A slope of -1 is indicated as a reference. Bottom left: semilog plot of top figure. Bottom right: semilog plot of magnetic spectra measured at point 3 in VKS (from Ref. [13]). The different curves correspond to different magnetic Reynolds numbers as indicated in the legend, with increasing Rm from light gray to black curves.

IV. MAGNETOHYDRODYNAMIC DYNAMO

We now turn to the case of the MHD dynamo and compare dynamical fluctuations observed in the VKS experiment and numerical results from the present TG simulations. Though parameters are not really comparable (in particular the Prandtl number differs by orders of magnitude as it is of the order of 6×10^{-6} in VKS while it is 0.5 in the simulation), experimental and numerical spectra of magnetic fluctuations show a remarkably good agreement, with in particular a wide $1/f$ range as shown in Fig. 8 (top), where we have plotted the magnetic spectra measured in the bulk at point 1 in VKS and in the simulation. As in the hydrodynamic case, this long-term memory is associated with the evolution of the large-scale modes. However, the magnetic field now appears to develop a $1/f$ regime over a much wider range of scales (almost 2 decades) than in the passively advected case. This indicates that the dynamo field develops its own long-term dynamics, which increases the correlation time scale as the magnetic field produced by the dynamo is spatially correlated at the largest available scale in the box. As a result, the range of time scales for which long-term memory is observed is substantially increased in the case of the self-sustained dynamo. This can be clearly seen in Fig. 9 which shows the temporal evolution of the axial position of the shear layer [Fig. 9(a)] and the corresponding spectrum [Fig. 9(b)]. From the temporal evolution we see that the transitions of the shear layer from one side of the box to the other occur over time scales much longer than what was previously observed in Fig. 6 for the purely hydrodynamic case. It can also be observed that intermittent periods of rapid fluctuations may appear during the long stable periods. This results in very a wide range of time scales involved in the overall dynamics, as revealed by the spectrum in Fig. 9(b), where it can be particularly noted that the $1/f$ regime extends towards much lower frequencies (longer time scales) than in the hydrodynamic case without even reaching a low-frequency plateau with the available length of the present simulations. Interestingly, we also note that the remarkable collapse of the experimental and numerical spectra in Fig. 8 (top) is obtained when the frequency in the simulation is normalized by $F_0 = u_{\mathrm{rms}}/2L$, with $L = \pi$ the forcing scale of the TG simulation and not by $F_0 = u_{\mathrm{rms}}/L$ as was the case

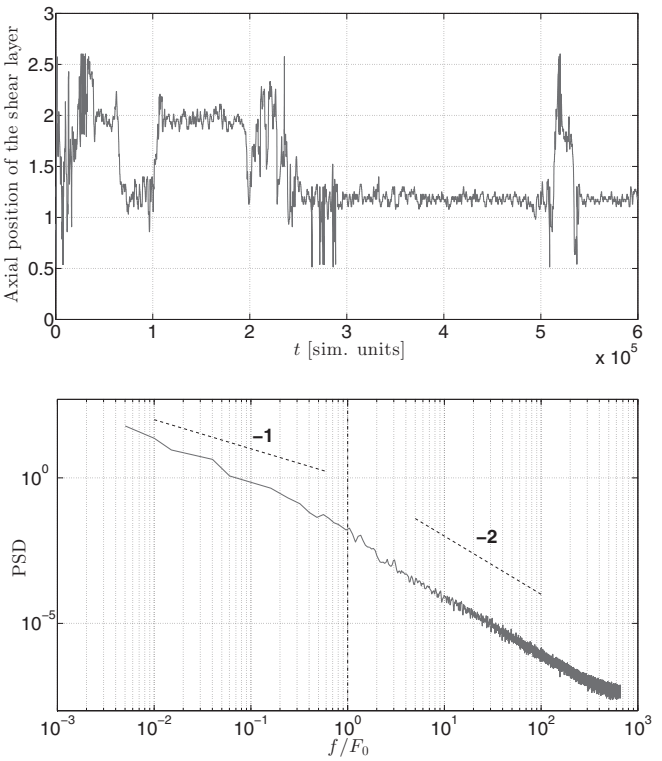

FIG. 9. Position of the shear layer as a function of time in the numerical simulations of dynamo action, and power spectrum of the signal. A slope of -1 is indicated as a reference.

for the passively advected magnetic field previously discussed. This is related to the large-scale correlation of the dynamo field, which is now correlated over the entire simulation box which is twice the forcing scale.

The existence of $1/f$ slow dynamics of magnetic fluctuations, related to the large-scale nature of magnetic field, seems to be a robust behavior of MHD large-scale dynamos. It is consistently observed in VKS experiment and TG simulations, which have similar flow geometries, but different boundary conditions, MHD parameters (mostly in terms of Prandtl numbers), and which have very likely different dynamo-generating mechanisms (VKS generates an axial dipole and is very sensitive to electromagnetic boundary conditions, while TG generates an equatorial dipole and operates in a homogeneous medium). A slow-dynamics $1/f$ regime has also been reported in the Karlsruhe dynamo experiment, which has a different geometry, different fluctuation levels, and different dynamo mechanism. In Ref. [14] it is argued from the results of a large number of numerical simulations that in systems that develop inverse cascades (as, e.g., helical MHD turbulence) the development of $1/f$ noise and long-term memory is more robust, in the sense that it is independent of details of the flow geometry and forcing. The present results are in good agreement with these arguments, and confirms in experiments the previous numerical results.

An interesting observation can also be done regarding the dissipative regime of the high-frequency magnetic spectra. As observed in Fig. 8 (top), this regime is not resolved in the experimental data, due to limitations in dynamical resolution of the magnetic measurements when performed in the bulk of the flow. However, the dissipation behavior can be better resolved from measurements in the outer layer of sodium, in the vicinity of the copper shell (for instance at point 3 in the VKS sketch in Fig. 1), where no flow is present and magnetic dynamics results essentially from diffusion processes of the turbulent magnetic fluctuations in the bulk. Such measurements show that the far dissipation spectrum of magnetic dynamo field decreases exponentially with the frequency f (as an example, the bottom right panel of Fig. 8 reproduces results from Fig. 16(c) in [13]). Though we do not have an explanation for such an exponential spectral regime, we interestingly find that the same exponential behavior is captured by the simulation as shown in Fig. 8 (bottom left panel). TG simulations therefore are able to reproduce a large number of temporal spectral properties of turbulent magnetic fluctuations as measured in the VKS experiment.

V. CONCLUSIONS

We presented a comparison of time series of pointwise measurements of the velocity and of the magnetic field, both from direct numerical simulations and from experiments of turbulence in conducting flows. Two configurations were considered: (1) a case with a weak externally imposed magnetic field, in which induction generated by fluid motions can be used as a tracer of the velocity field (and mostly of the large-scale modes of the velocity field, as the magnetic Prandtl number considered in that case is small), and (2) a case with self-sustained magnetic fields. The flow in the experiment corresponds to a von Kármán swirling flow between two counterrotating impellers in a cylindrical vessel, while in the simulations the flow is generated in a square box using periodic Taylor-Green forcing.

While experiments excel at providing time statistics of field fluctuations with limited spatial information of the flow geometry, numerical simulations tend to be performed at high resolution for short times, thus providing substantial amounts of spatial information with little time statistics. In the present study a different approach was used, considering low-resolution simulations but extended for very long times, so comparisons between experimental and numerical data can be done on the same grounds.

Good general agreement was found between spectral properties in simulations and experiments, both in the hydrodynamic (weak imposed magnetic field) and dynamo cases. Intermediate and high frequency spectra from the experiments were found to be well reproduced by the simulations. In particular, evidence of long-term memory and $1/f$ noise at intermediate frequencies was found in both experiments and simulations. In the hydrodynamic case, low-frequency magnetic spectra were found to deviate between the experiment and the simulation. This can be attributed to different induction processes operating in the bounded experiment and in the periodic simulations.

In the hydrodynamic regime, $1/f$ noise in the kinetic spectrum is a signature of the slow fluctuations of the largest structures of the flow, and particularly of the midplane shear

layer. As a consequence, this is only observed in the simulation when small wave numbers are selected. This selection is naturally operated when considering magnetic fluctuations of a passively advected magnetic field in low Prandtl number situations, which are indeed found to exhibit $1/f$ behavior.

In the dynamo case, $1/f$ noise of magnetic field fluctuations is enhanced over a wider range of scales, which is attributable to the intrinsic large-scale nature of the generated field. The remarkable collapse of simulations (at $\mathrm{Pm} = 0.5$) and experiments (at $\mathrm{Pm} \approx 10^{-5}$) indicates that this may be a fundamental and robust property of large-scale MHD dynamos where slow fluctuations (both kinematic and magnetic) appear when the magnetic and velocity field become intimately coupled. This last conclusion may be particular useful to extrapolate dynamical behaviors from simulations at $\mathrm{Pm} \approx 1$ (a condition computationally favorable) to more realistic dynamos (natural or experimental) at small Prandtl regimes (which are computationally expensive to simulate). A particular example where this may be relevant is the case of dynamo reversals, which take place on very long time scales and which cannot be studied in simulations at low magnetic Prandtl number.

The reasons why the $1/f$ scaling ends at a given (very low) frequency are not clear. In the hydrodynamic case, it has been observed in experiments [2,18] that this cutoff can be associated with the existence of a characteristic time scale for the slow instability of the midplane shear layer. In the experiments and simulations of magnetic induction, as mentioned above, the boundary conditions affect the extension of the $1/f$ spectrum in the magnetic field. Finally, in the dynamo regime that has a much longer memory, the finite length of the simulations introduces an artificial cutoff at low frequencies, as no clear plateau can be observed for the lowest frequencies resolved.

ACKNOWLEDGMENTS

The authors acknowledge support from grant ECOS A08U02. P.D.M. and P.D. acknowledge support from Grants No. PIP 11220090100825, No. UBACYT 20020110200359, No. PICT 2011-1529, and No. PICT 2011-1626. The French authors acknowledge their colleagues of the VKS team with whom experimental data have been obtained. Their work was supported by ANR 08-0039-02.

[1] A. de la Torre and J. Burguete, Phys. Rev. Lett. **99**, 054101 (2007).
[2] E. Crespo Del Arco, J. J. Sanchez-Alvarez, E. Serre, A. De La Torre, and J. Burguete, Geophys. Astrophys. Fluid Dyn. **103**, 163 (2009).
[3] E. W. Montroll and M. F. Shlesinger, Proc. Natl. Acad. Sci. USA **79**, 3380 (1982).
[4] S. Machlup, in *Sixth International Conference on Noise in Physical Systems*, edited by P. H. E. Meijer, R. D. Mountain, and R. J. Soulen (National Bureau of Standards, Washington, DC, 1981), pp. 157–160.
[5] Y. Ponty, H. Politano, and J. F. Pinton, Phys. Rev. Lett. **92**, 144503 (2004).
[6] P. Dmitruk and W. H. Matthaeus, Phys. Rev. E **76**, 036305 (2007).
[7] M. Goldstein, D. Roberts, and W. Matthaeus, Annu. Rev. Astron. Astrophys. **33**, 283 (1995).
[8] W. H. Matthaeus and M. L. Goldstein, Phys. Rev. Lett. **57**, 495 (1986).
[9] W. H. Matthaeus, B. Breech, P. Dmitruk, A. Bemporad, G. Poletto, M. Velli, and M. Romoli, Astrophys. J. **657**, L121 (2007).
[10] V. Carbone, L. Sorriso-Valvo, A. Vecchio, F. Lepreti, P. Veltri, P. Harabaglia, and I. Guerra, Phys. Rev. Lett. **96**, 128501 (2006).
[11] L. Ziegler and C. Constable, Earth Planet. Sci. Lett. **312**, 300 (2011).
[12] C. Constable and C. Johnson, Phys. Earth Planet. Inter. **153**, 61 (2005).
[13] R. Monchaux, M. Berhanu, S. Aumaitre, A. Chiffaudel, F. Daviaud, B. Dubrulle, F. Ravelet, S. Fauve, N. Mordant, F. Petrelis *et al.*, Phys. Fluids **21**, 035108 (2009).
[14] P. Dmitruk, P. D. Mininni, A. Pouquet, S. Servidio, and W. H. Matthaeus, Phys. Rev. E **83**, 066318 (2011).
[15] P. Mininni, Annu. Rev. Fluid Mech. **43**, 377 (2011).
[16] R. Volk, P. Odier, and J.-F. Pinton, Phys. Fluids **18**, 085105 (2006).
[17] G. Verhille, N. Plihon, M. Bourgoin, P. Odier, and J.-F. Pinton, Space Sci. Rev. **152**, 543 (2010).
[18] M. López-Caballero and J. Burguete, Phys. Rev. Lett. **110**, 124501 (2013).
[19] G. Verhille, R. Khalilov, P. Frick, N. Plihon, and J.-F. Pinton, J. Fluid Mech. **693**, 243 (2012).
[20] V. Noskov, R. Stepanov, S. Denisov, P. Frick, G. Verhille, N. Plihon, and J.-F. Pinton, Phys. Fluids **21**, 045108 (2009).
[21] Y. Ponty, P. D. Mininni, D. C. Montgomery, J.-F. Pinton, H. Politano, and A. Pouquet, Phys. Rev. Lett. **94**, 164502 (2005).
[22] P. Mininni, Y. Ponty, D. Montgomery, J. Pinton, H. Politano, and A. Pouquet, Astrophys. J. **626**, 853 (2005).
[23] D. Gomez, P. Mininni, and P. Dmitruk, Phys. Scr. **T116**, 123 (2005).
[24] D. Gomez, P. Mininni, and P. Dmitruk, Advances in Space Research **35**, 899 (2005).
[25] P. D. Mininni, D. Rosenberg, R. Reddy, and A. Pouquet, Parallel Computing **37**, 316 (2011).
[26] M. Bourgoin, P. Odier, J.-F. Pinton, and Y. Ricard, Phys. Fluids **16**, 2529 (2004).
[27] F. Ravelet, A. Chiffaudel, and F. Daviaud, J. Fluid Mech. **601**, 339 (2008).
[28] M. Bourgoin, R. Volk, P. Frick, S. Khripchenko, P. Odier, and J.-F. Pinton, Magnetohydrodynamics **40**, 13 (2004).